ResearchGate

See discussions, stats, and author profiles for this publication at: https://www.researchgate.net/publication/260241730

# Density functional theory study of small X-doped Mgn (X = Fe, Co, Ni, n=1–9) bimetallic clusters: Equilibrium structures, stabilities, electronic and magnetic properties

**ARTICLE** *in* JOURNAL OF MOLECULAR MODELING · MARCH 2014

Impact Factor: 1.74 · DOI: 10.1007/s00894-014-2087-x · Source: PubMed

CITATION
1

READS
77

**2 AUTHORS:**

Fanjie Kong
Yancheng Institute of Technology
**32** PUBLICATIONS **79** CITATIONS
SEE PROFILE

Yan-Fei Hu
Sichuan University of Science and Engineer…
**16** PUBLICATIONS **25** CITATIONS
SEE PROFILE

Available from: Fanjie Kong
Retrieved on: 24 January 2016

# *Density functional theory study of small X-doped $Mg_n$ (X = Fe, Co, Ni, n=1–9) bimetallic clusters: equilibrium structures, stabilities, electronic and magnetic properties*

**Fanjie Kong & Yanfei Hu**

**Journal of Molecular Modeling**
Computational Chemistry - Life Science - Advanced Materials - New Methods

ISSN 1610-2940
Volume 20
Number 3

J Mol Model (2014) 20:1-10
DOI 10.1007/s00894-014-2087-x

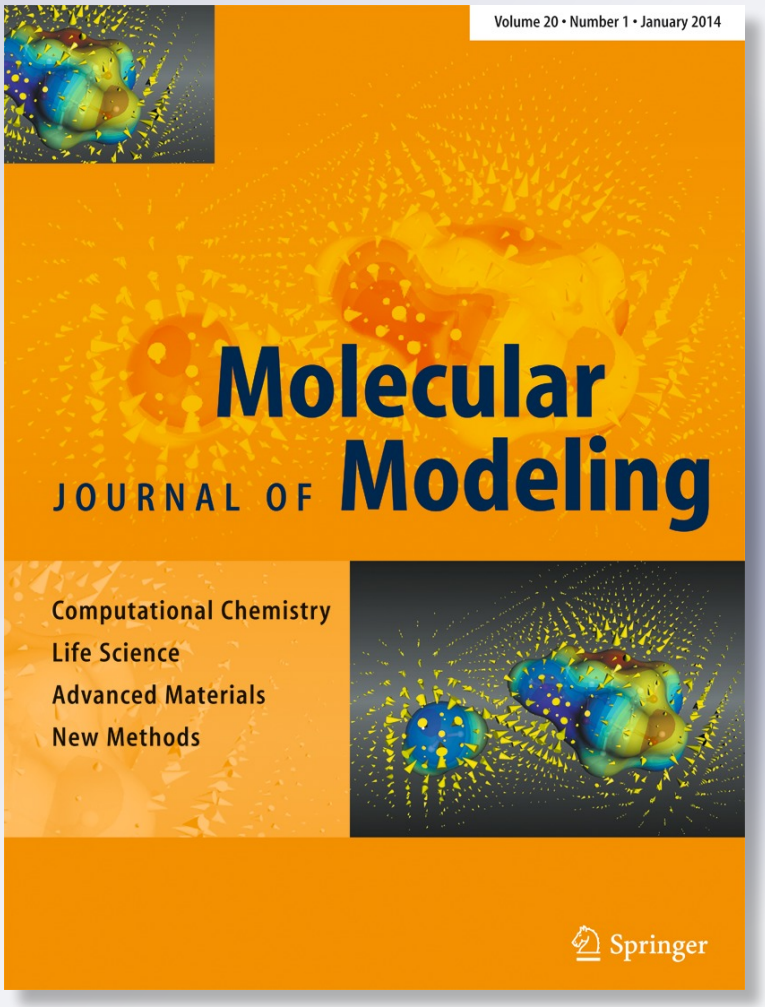


Springer

Your article is protected by copyright and all rights are held exclusively by Springer-Verlag Berlin Heidelberg. This e-offprint is for personal use only and shall not be self-archived in electronic repositories. If you wish to self-archive your article, please use the accepted manuscript version for posting on your own website. You may further deposit the accepted manuscript version in any repository, provided it is only made publicly available 12 months after official publication or later and provided acknowledgement is given to the original source of publication and a link is inserted to the published article on Springer's website. The link must be accompanied by the following text: "The final publication is available at link.springer.com".

Author's personal copy

J Mol Model (2014) 20:2087
DOI 10.1007/s00894-014-2087-x

ORIGINAL PAPER

# Density functional theory study of small X-doped $Mg_n$ (X = Fe, Co, Ni, $n$=1–9) bimetallic clusters: equilibrium structures, stabilities, electronic and magnetic properties

**Fanjie Kong · Yanfei Hu**

Received: 10 August 2013 / Accepted: 19 November 2013
© Springer-Verlag Berlin Heidelberg 2014

**Abstract** The geometries, stabilities, and electronic and magnetic properties of $Mg_nX$ (X = Fe, Co, Ni, $n$=1–9) clusters were investigated systematically within the framework of the gradient-corrected density functional theory. The results show that the $Mg_nFe$, $Mg_nCo$, and $Mg_nNi$ clusters have similar geometric structures and that the X atom in $Mg_nX$ clusters prefers to be endohedrally doped. The average atomic binding energies, fragmentation energies, second-order differences in energy, and HOMO–LUMO gaps show that $Mg_4X$ (X = Fe, Co, Ni) clusters possess relatively high stability. Natural population analysis was performed and the results showed that the 3*s* and 4*s* electrons always transfer to the 3*d* and 4*p* orbitals in the bonding atoms, and that electrons also transfer from the Mg atoms to the doped atoms (Fe, Co, Ni). In addition, the spin magnetic moments were analyzed and compared. Several clusters, such as $Mg_{1,2,3,4,5,6,8,9}Fe$, $Mg_{1,2,4,5,6,8,9}Co$, and $Mg_{1,2,5,6,7,9}Ni$, present high magnetic moments (4 $\mu_B$, 3 $\mu_B$, and 2 $\mu_B$, respectively).

**Keywords** $Mg_nX$ (X = Fe, Co, Ni, $n$=1–9) clusters · Density functional theory · Structure stability · Magnetic property

## Introduction

Metal clusters have been investigated extensively over the last two decades due to their potential applications in physical and chemical fields. In theory, the jellium model successfully explains the electronic structures and magic number structures of some pure and doped metal clusters [1]. Magnesium is a good hydrogen storage material due to its light weight, low cost, cyclability, and high H-storage capacity (7.6 % by weight) once the hydride $MgH_2$ is formed. Mechanically alloying Mg with transition metals (TMs) such as Ni, Fe, V, or Pd allows these metals to be mixed together into a nanocomposite structure [2, 3]. In particular, alloying Mg with TMs can slightly improve the thermodynamic properties of the hydride by favoring $H_2$ adsorption/dissociation and consequent atomic hydrogen absorption/desorption due to a weakening of the bonding between Mg and H atoms. Therefore, it is essential to investigate the effect of transition metal doping on the structural and electronic properties of the Mg cluster.

Reuse et al. performed electronic structure calculations on neutral, anionic, cationic, and doubly ionized $Mg_n$ ($n$≤7) clusters to examine the effect of charge on the geometries and stabilities of these clusters [4]. One of the main conclusions that could be drawn from their work is that $Mg_n$ clusters have a strong tendency to form compact structures; that is, most of the neutral, anionic, and singly ionized species tend to form the maximum number of bonds possible. Kumar et al. studied the structure, growth, and bonding characteristics of $Mg_n$ ($n$=2–13) clusters and found that tetrahedral and trigonal prismatic structures are two important base constituents of the structures of $Mg_n$ clusters, to which atoms can be added by capping the faces [5]. In addition, they suggested that $Mg_n$ clusters show mixed bonding character and an oscillatory and slow convergence to bulk metallic behavior. Gong et al. revealed that the number of 3*p* electrons involved in *sp* hybridization increases as the cluster size increases by systematically investigating the electronic structures of magnesium clusters containing up to 57 atoms [6]. Kaplan et al. concluded that alkaline-earth dimers ($Be_2$, $Mg_2$, and $Ca_2$) can be considered van der Waals molecules, while the binding present in

F. Kong (✉)
Department of Physics, Yancheng Institute of Technology, Yancheng 224051, China
e-mail: fanjiekong@gmail.com

Y. Hu
School of Science, Sichuan University of Science and Engineering, Zigong 643000, China

Published online: 18 February 2014

Author's personal copy



alkaline-earth trimers ($Be_3$, $Mg_3$, and $Ca_3$) is a mixture of physical (van der Waals) and chemical (nonadditive exchange). Furthermore, a natural bond orbital (NBO) analysis revealed a relatively large *p* population in all of the clusters [7]. Akola et al. observed that the onset of metallization of $Mg_n$ clusters is difficult to assign, since both the *sp* hybridization and the energy gap between the valence band and the conduction band do not evolve rapidly towards known bulk properties [8]. Concerning the issue of a possible electronic structure transition from a phase with localized electrons to one with delocalized electrons, Thomas Diederich presented the first proof of a transition to electron delocalization in free $Mg_n$ clusters, i.e., evidence of the onset of an electronic shell structure [9]. The energetic and structural properties of neutral $Mg_n$ clusters ($n$=2–22 and selected clusters up to 309) have been investigated by means of density functional theory. Small clusters with $n$=4, 10, and 20 show enhanced stability, which is in line with the predictions of the shell model. Larger clusters were selected according to the principle of geometric shell closure, and different kinds of shapes and packing types were considered [10]. Owen C. Thomas measured the photoelectron spectra of mass-selected $Mg_n$ cluster anions over the size range $n$=3–35. The *s*–*p* band gap was observed to be narrow for $n$=18, signaling the onset of metallic behavior. An electronic shell structure was inferred from gap "reopenings" and mass-spectral magic numbers [11]. The binding energies of the two most external electrons in $Mg_n$ ($n$=2–22) clusters were computed. The results were compared with photoelectron spectroscopy data, and their implications for the finite-size analog of the nonmetal-to-metal transition were analyzed [12]. The geometries of neutral and singly charged $Mg_n$ clusters consisting of up to 21 atoms were optimized, and the electronic shell closures, binding energies per atom, ionization potentials, and the gaps between the highest occupied and the lowest unoccupied molecular orbitals (HOMO–LUMO gaps) were studied systematically. The hexagonal close-packed (hcp) structures and the metallic evolutions of $Mg_n$ clusters were observed, and the stabilities of linear chains and rings of the Mg atoms were discussed [13]. The abundance distribution of $Mg_n$ clusters can be explained by the presence of an electronic shell structure. The associated metallic bonding was observed at about $n$=20 atoms. Electronic level crossing at the highest occupied molecular orbital that results in additional magic numbers was resolved [14]. The structural and electronic properties of $Mg_n$ clusters for the size range $n$=10–56 were explored using the minima hopping global geometry optimization method on the density functional potential energy surface. This revealed that most of the global minima are asymmetric beyond $n$=20 and that the growth follows a peculiar cyclic pattern where the core and surface grow alternately for $n$>20 [15].

The electronic structures and stabilities of $XMg_8$ clusters (X = Be, B, C, N, O, and F) have been studied using first-principles calculations to understand the variations in the bonding within heteroatomic clusters that mix simple divalent metals with main-group dopants [16]. A single transition metal element doped into an *sp* metal host constitutes an ideal classical system for studying the interaction of *d* electrons with a nearly free electron gas and the local magnetic moment. However, less attention has been paid to doped $Mg_n$ clusters with TMs.

The aim of the work described in the present paper was to investigate the structural, electronic, and magnetic properties of a wide range of 3*d* TM-doped $Mg_n$ clusters: $Mg_nX$ (M = Fe, Co, Ni, $n$=1–9). We focused on the effect of transition metal doping on the structural and electronic properties of the Mg cluster, how the magnetic properties of the cluster change as the local electrons of an isolated atom begin to delocalize in an $Mg_nX$ cluster, and how the magnetism of $Mg_nX$ clusters varies with increasing cluster size.

## Computational details

In this work, we systematically investigated the properties of X-doped $Mg_n$ (X = Fe, Co, Ni, $n$=1–9) clusters using density functional theory based on the hybrid Becke-type three-parameter exchange functional [17] paired with the gradient-corrected Perdew–Wang 91 correlation functional (B3PW91) [18]. All electron calculations were carried out using the 6-311+G basis set [19–21]. To evaluate the accuracy of the selected scheme at describing $Mg_nX$ clusters, we first carried out benchmark calculations of $Mg_2$, $Fe_2$, $Co_2$, and $Ni_2$ dimers. The calculated results as well as the available experimental values for the equilibrium bond lengths, dissociation energies, and harmonic vibrational frequencies are summarized in Table 1. The calculated values are in good agreement with the experimental results and those from other available theoretical works [22–38]. The predicted equilibrium bond length for the $Mg_2$ dimer is 3.683 Å. Although this deviates slightly from the experimental value of 3.891 Å, it is in excellent agreement with previous theoretical values (3.68 Å) [39]. The bond length of the $Mg_2$ dimer is longer than those of the $Fe_2$, $Co_2$, and $Ni_2$ dimers. It is interesting to note that the dissociation energies of the $Fe_2$, $Co_2$, and $Ni_2$ dimers are larger than that of the $Mg_2$ dimer.

The initial search for all possible low-lying isomers of pure $Mg_n$ clusters was carried out manually due to the small number of possible structures to be considered during geometry optimizations. For $Mg_nX$ (X = Fe, Co, Ni, $n$=1–9) clusters, the possible initial isomers were constructed by substituting one X for an Mg atom in the host $Mg_n$ cluster or by placing the X atom at each possible site of the $Mg_{n-1}$ cluster. Furthermore, vibrational frequency calculations were performed to guarantee that the optimized structures corresponded to local minima on the multidimensional

Author's personal copy



**Table 1** The computed bond lengths ($r_e$), dissociation energies ($D_e$), and vibrational frequencies ($\omega_e$) of the $Mg_2$, $Fe_2$, $Co_2$, and $Ni_2$ dimers

| | | $r_e$ (Å) | $D_e$ (eV) | $\omega_e$ ($cm^{-1}$) |
|---|---|---|---|---|
| $Mg_2$ | B3PW91/6-311+G | 3.683 | 0.0615 | 77.9 |
| | Experiment | 3.891[a] | 0.0886[a], 0.025[b] | / |
| $Fe_2$ | B3PW91/6-311+G | 2.117 | 1.147 | 305.5 |
| | Experiment | 2.02±0.02[c,d,e], 1.87±0.13[f], 1.85[g] | 1.3[c,d,e], 1.14[g], 1.15±0.09[h] | 299.6[i], 300[c,d,f,g], 299.7[i] |
| $Co_2$ | B3PW91/6-311+G | 2.201 | 1.651 | 299.0 |
| | Experiment | / | 1.69±0.26[j] | 280±20[k], 290[k], 296.8±0.54[l] |
| $Ni_2$ | B3PW91/6-311+G | 2.151 | 2.055 | 293.8 |
| | Experiment | 2.155±0.01[m], 2.12[m], 2.1545±0.0004[n] | 2.068±0.01[m], 2.20[m] | 330[o], 380.9[p], 259.2±3.0[q] |

[a] From [21]
[b] From [22]
[c] From [23]
[d] From [24]
[e] From [25]
[f] From [26]
[g] From [27]
[h] From [28]
[i] From [29]
[j] From [30]
[k] From [31]
[l] From [32]
[m] From [33]
[n] From [34]
[o] From [35]
[p] From [36]
[q] From [37]

potential-energy surface and to provide the zero-point energy (ZPE). Every initial configuration with various possible spin multiplicities was optimized at the B3PW91 level. The structures with the lowest energies were chosen as the ground-state configurations. The default self-consistent convergence to $10^{-8}$ a.u. was used, which was exact enough to ensure that the results are valid. All calculations were performed using the Gaussian 09 package [40].

## Results and discussion

### Geometric structures

For $Mg_nX$ (X = Fe, Co, Ni, $n$=1–9) clusters, a great number of initial possible geometries with various possible spin multiplicities were optimized. Only the lowest-energy structure for each $Mg_nX$ cluster is shown in Fig. 1. Meanwhile, the electronic states, symmetries, spin multiplicities, HOMO energies, LUMO energies, as well as vibrational frequencies of the $Mg_nX$ (X = Fe, Co, Ni, $n$=1–9) clusters are listed in Table 2.

#### *Pure $Mg_n$ (n= 1–10) clusters*

In order to explore the effect of TM doping on the stabilities and properties of pure $Mg_n$ clusters, the energetically lowest-lying configurations of the $Mg_n$ ($n$=1–10) clusters were first optimized and obtained at the B3PW91/6-311+G level. Taking lots of possible initial structures into account, the most stable isomers for each size are shown in Fig. 1. From Fig. 1, we can see that the most stable structures of pure $Mg_n$ ($n$=3–10) clusters are triangular, tetrahedral, trigonal bipyramidal, fused tetrahedral, pentagonal bipyramidal, capped pentagonal bipyramidal, tricapped trigonal prismatic, and tetracapped trigonal prismatic, respectively, in good agreement with previous results [12, 15]. In addition, the average atomic binding energies, fragmentation energies, second-order differences in energy, HOMO–LUMO gaps, and magnetic moments of $Mg_n$ clusters were also studied and compared with $Mg_nX$ (X = Fe, Co, Ni, $n$=1–9) clusters.

#### *X-doped $Mg_n$ (X= Fe, Co, Ni, n= 1–9) clusters*

It was found that the bond lengths of the MgX (X = Fe, Co, Ni) clusters gradually decrease in the order Fe > Ni > Co. For

Author's personal copy



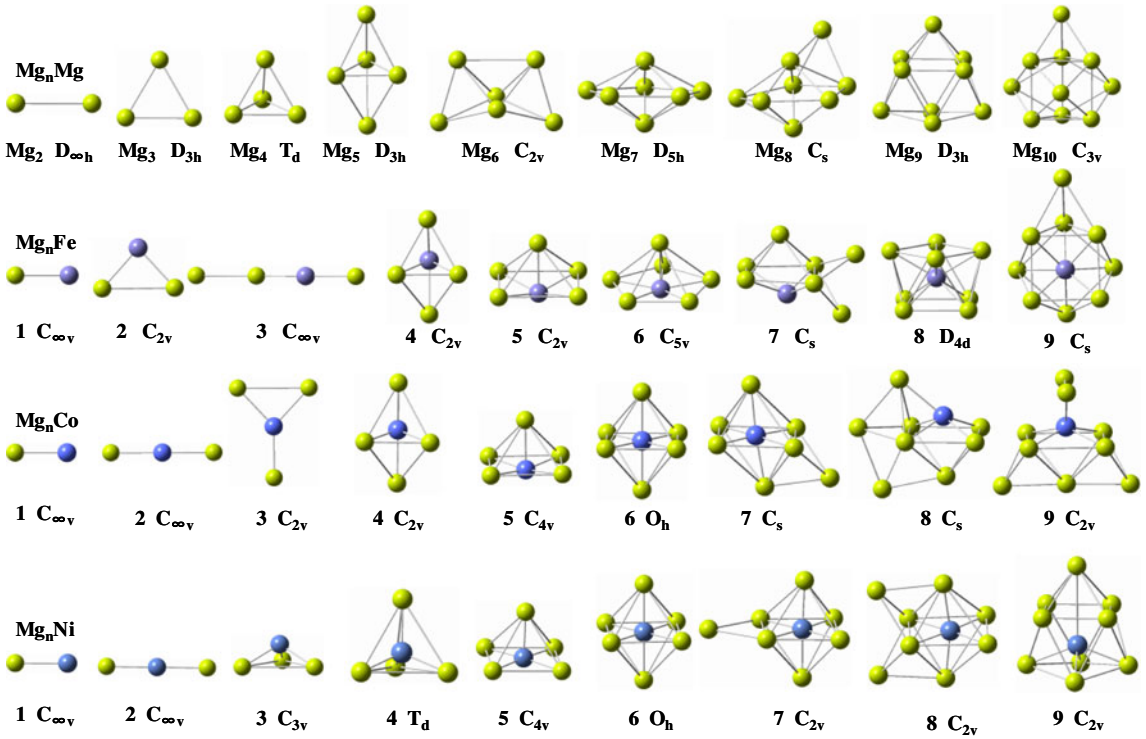


**Fig. 1** Lowest-energy structures for $Mg_{n+1}$ and $Mg_nX$ (X = Fe, Co, Ni, $n$=1–9) clusters. The *yellow* and *blue balls* represent Mg and X atoms, respectively

the $Mg_2X$ (X = Fe, Co, Ni) clusters, the global minimum structure of $Mg_2Fe$ is isosceles trigonal with $C_{2v}$ symmetry, in which Fe is connected to two Mg atoms. The structures of the $Mg_2Co$ and $Mg_2Ni$ clusters are linear with $C_{\infty v}$ symmetry, where the Co and Ni atoms sit between the two Mg atoms. The structures of the $Mg_3X$ vary significantly for different TM atoms. The $Mg_3Fe$ cluster possesses a linear structure with $C_{\infty v}$ symmetry, the $Mg_3Co$ cluster shows a planar Y-shaped structure with $C_{2v}$ symmetry, while the $Mg_3Ni$ cluster presents a three-dimensional (3D) tetrahedral configuration which can be obtained by adding one Ni atom along the $C_3$ axis of the triangular $Mg_3$ cluster ($D_{3h}$). The structure of $Mg_3Ni$ can also be regarded as a doped structure that is based on the tetrahedral $Mg_4$ cluster (i.e., it is created by substituting one Mg atom with an Ni atom). Starting from $n$=4, the ground-state structures of the $Mg_nX$ (X = Fe, Co) clusters show 3D geometries. The symmetries of the $Mg_4Fe$ and $Mg_4Co$ clusters are identical ($C_{2v}$), and the structures can be obtained by substituting one Mg atom in the isosceles triangle of a trigonal bipyramidal $Mg_5$ cluster with an Fe or Co atom, respectively. The ground-state structure of the $Mg_4Ni$ cluster with the electron state $^1A_1$ and $T_d$ symmetry can be generated by inserting the Ni atom at the tetrahedral interstitial site of the $Mg_4$ cluster. The ground-state structure of $Mg_5Ni$ is a square pyramidal arrangement in which the Ni atom is located in the middle of the square unit, while the ground-state configurations of $Mg_5Fe$ and $Mg_5Co$ are capped square pyramids, with the Fe and Co atoms located in the center of the square face. A pentagonal pyramidal arrangement with the Fe located in the center of the pentagon is the global minimum of the $Mg_6Fe$ cluster. The most stable structures of $Mg_6Co$ and $Mg_6Ni$ are square bipyramids in which the Co or Ni atom, respectively, is at the center of the square. The global minimum of the $Mg_7X$ cluster can be generated by adding an Mg atom to the corresponding $Mg_6X$ cluster. The motif of the $Mg_8Fe$ cluster looks quite like that of the $Mg_9$ cluster but with the top Mg atom removed, and the Fe atom located at the central position of the cluster. The most stable structures of the $Mg_8Co$ and $Mg_8Ni$ clusters can be obtained by adding an Mg atom to the $Mg_7Co$ and $Mg_7Ni$ clusters, respectively, which have similar structures; however, they possess different symmetries ($C_s$, $C_{2v}$) and electronic states ($^4A''$, $^1A_1$). For $Mg_9X$ clusters, possible initial structural configurations and spin states were considered to localize the ground-state structure. As a result, the lowest-energy structure of $Mg_9Fe$ can be related to the $Mg_{10}$ cluster but with the inner Mg atom replaced with one Fe atom. The 3D structure of $Mg_9Co$ with a symmetry of $C_{2v}$ is the lowest-energy structure; this can be obtained by adding two Mg atoms to the $Mg_7Co$ cluster. Also, the ground-state structure of $Mg_9Ni$ can be viewed as the result of inserting one Ni atom into the 3D structure of $Mg_9$, with the Ni atom localizing inside the cluster.

From the above discussion, it is clear that the X atom tends to reside at the center of the doped $Mg_n$ cluster, leading to an

Author's personal copy



**Table 2** Electronic states, symmetries, spin multiplicities, HOMO energies, LUMO energies, and vibrational frequencies of the $Mg_nX$ (X = Fe, Co, Ni, $n$=1–9) clusters

| Cluster | State | Symm | Multi | HOMO (hartrees) | LUMO (hartrees) | Frequency ($cm^{-1}$) |
|---|---|---|---|---|---|---|
| MgFe | / | $C_{\infty v}$ | 5 | −0.15425 | −0.07835 | 193.1 |
| $Mg_2Fe$ | $^5B_1$ | $C_{2v}$ | 5 | −0.15886 | −0.08574 | 77.1, 162.0, 192.1 |
| $Mg_3Fe$ | $^5\Sigma$ | $C_{\infty v}$ | 5 | −0.13636 | −0.07681 | 24.6, 68.0, 95.8, 175.1, 230.5 |
| $Mg_4Fe$ | $^5A_2$ | $C_{2v}$ | 5 | −0.15827 | −0.08920 | 64.4, 95.6, 140.1, 142.8, 174.9 |
| $Mg_5Fe$ | $^5B_1$ | $C_{2v}$ | 5 | −0.14934 | −0.09632 | 38.6, 66.4, 75.9, 80.0, 85.0 |
| $Mg_6Fe$ | $^5A_1$ | $C_{5v}$ | 5 | −0.15551 | −0.10065 | 58.3, 76.4, 92.8, 127.4, 157.7 |
| $Mg_7Fe$ | $^3A'$ | $C_s$ | 3 | −0.14848 | −0.10723 | 20.0, 35.3, 61.8, 77.7, 103.0 |
| $Mg_8Fe$ | $^5A_1$ | $D_{4d}$ | 5 | −0.14393 | −0.08718 | 50.0, 100.0, 117.3, 130.7, 144.0 |
| $Mg_9Fe$ | $^5A$ | $C_1$ | 5 | −0.14480 | −0.09114 | 41.8, 43.5, 62.5, 74.4, 95.4 |
| MgCo | / | $C_{\infty v}$ | 4 | −0.15976 | −0.08070 | 208.2 |
| $Mg_2Co$ | / | $C_{\infty v}$ | 4 | −0.14395 | −0.07847 | 43.8, 168.1, 193.6 |
| $Mg_3Co$ | $^2A_2$ | $C_{2v}$ | 2 | −0.13815 | −0.09118 | 33.4, 37.4, 49.4, 160.0, 166.2 |
| $Mg_4Co$ | $^4B_2$ | $C_{2v}$ | 4 | −0.15366 | −0.09435 | 54.0, 63.4, 93.0, 106.4, 121.1 |
| $Mg_5Co$ | $^4A$ | $C_1$ | 4 | −0.14398 | −0.08864 | 72.5, 74.6, 77.8, 82.9, 93.0 |
| $Mg_6Co$ | $^4A_{1g}$ | $O_h$ | 4 | −0.13899 | −0.08216 | 87.9, 118.2, 126.9, 215.7, 246.2 |
| $Mg_7Co$ | $^2A''$ | $C_s$ | 2 | −0.14206 | −0.08986 | 32.2, 55.5, 78.8, 86.1, 102.6 |
| $Mg_8Co$ | $^4A''$ | $C_s$ | 4 | −0.14646 | −0.09711 | 35.7, 36.4, 51.1, 67.3, 69.9 |
| $Mg_9Co$ | $^4A$ | $C_1$ | 4 | −0.14959 | −0.10578 | 66.0, 71.1, 84.0, 95.9, 104.5 |
| MgNi | $^3\Sigma$ | $C_{\infty v}$ | 3 | −0.16004 | −0.08474 | 206.3 |
| $Mg_2Ni$ | / | $C_{\infty v}$ | 3 | −0.14457 | −0.08198 | 42.4, 178.0, 201.3 |
| $Mg_3Ni$ | $^1A_1$ | $C_{3v}$ | 1 | −0.16736 | −0.09007 | 80.6, 254.0, 260.1, |
| $Mg_4Ni$ | $^1A_1$ | $T_d$ | 1 | −0.17448 | −0.08337 | 32.1, 64.2, 226.8, 289.0 |
| $Mg_5Ni$ | $^3A_2$ | $C_{4v}$ | 3 | −0.14048 | −0.09005 | 45.3, 70.3, 87.5, 102.9, 244.5 |
| $Mg_6Ni$ | $^3A_{1g}$ | $O_h$ | 3 | −0.12634 | −0.10393 | 58.7, 70.8, 97.4, 249.0, 306.0 |
| $Mg_7Ni$ | $^3A_1$ | $C_{2v}$ | 3 | −0.13350 | −0.09446 | 33.3, 65.9, 68.5, 73.8, 75.8 |
| $Mg_8Ni$ | $^1A_1$ | $C_{2v}$ | 1 | −0.15176 | −0.08771 | 57.0, 65.8, 71.8, 85.8, 98.6 |
| $Mg_9Ni$ | $^3A_2$ | $C_{2v}$ | 3 | −0.15619 | −0.10433 | 59.0, 74.3, 92.5, 93.7, 108.1 |

increased number of X–Mg bonds. However, if a large X atom is placed at the center of the cluster, the $Mg_nX$ cluster will undergo slight expansion, leading to an increase in the Mg–Mg bond length. The presence of such a central dopant in an $Mg_nX$ could easily increase the energies of the Mg–Mg bonds. The Fe, Co, and Ni dopant atoms dramatically affect the ground-state geometries of the $Mg_n$ clusters. Furthermore, the optimized geometries reveal that the substitution of an Mg atom with X and the capping of one Mg atom in an $Mg_{n-1}X$ cluster are the dominant growth patterns for $Mg_nX$ clusters.

## Relative stability

In order to gauge the relative stabilities and size-dependent behavior of the $Mg_nX$ clusters, we plotted the average binding energies $E_b(n)$, the fragmentation energies $\Delta_1E(n)$, and the second-order differences in the total energy $\Delta_2E(n)$ for the ground-state structures of $Mg_{n+1}$ and $Mg_nX$ (X = Fe, Co, Ni, $n$=1–9) clusters (see Figs. 2 and 3), which allowed us to gain insight into the variations in those parameters.

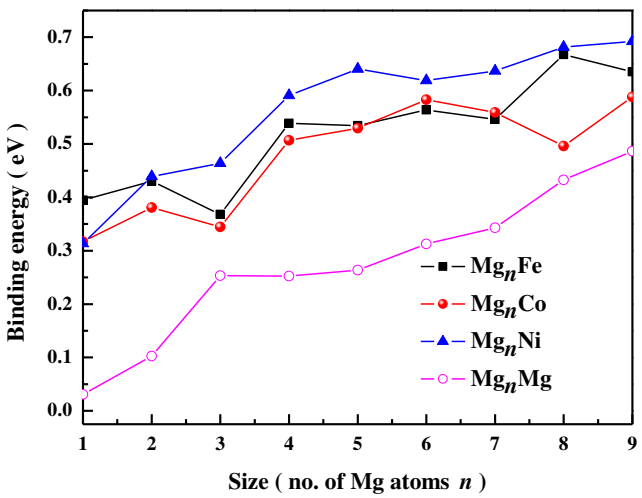


**Fig. 2** Size dependences of the average binding energies of $Mg_{n+1}$ and $Mg_nX$ (X = Fe, Co, Ni, $n$=1–9) clusters

Author's personal copy



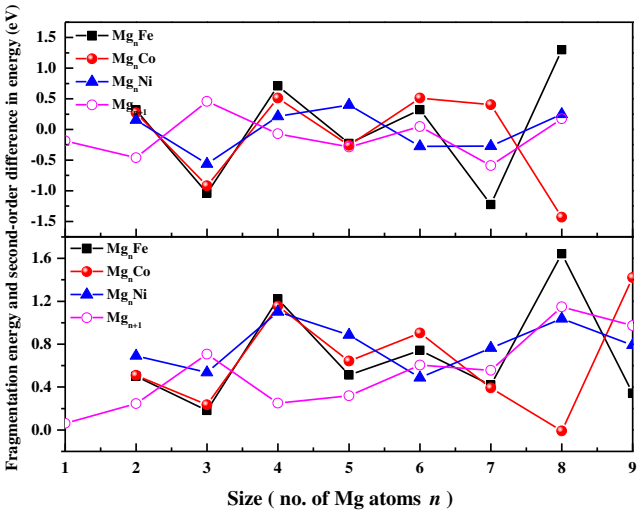


**Fig. 3** Size dependences of the fragmentation energies and the second-order differences in energies of $Mg_{n+1}$ and $Mg_nX$ (X = Fe, Co, Ni, $n$=1–9) clusters

For $Mg_nX$ (X = Fe, Co, Ni, $n$=1–9) clusters, $E_b(n)$, $\Delta_1E(n)$, and $\Delta_2E(n)$ are defined as follows:

$$E_b(n) = \frac{E(X) + nE(Mg) - E(Mg_nX)}{n+1} \quad (1)$$

$$\Delta_1E(n) = E(Mg_{n-1}X) + E(Mg) - E(Mg_nX) \quad (2)$$

$$\Delta_2E(n) = E(Mg_{n-1}X) + E(Mg_{n+1}X) - 2E(Mg_nX). \quad (3)$$

Here, $E$ is the total energy of the corresponding system.

From Fig. 2, it is clear that the average atomic binding energies of both pure and X-doped magnesium clusters increase as the cluster size increases. Slight oscillations are seen in the binding energies of $Mg_{n+1}$ and $Mg_nX$ (X = Fe, Co, Ni, $n$=1–9) clusters. There are several local peaks corresponding to $Mg_4Fe$, $Mg_6Fe$, $Mg_8Fe$, $Mg_2Co$, $Mg_6Co$, and $Mg_5Ni$, respectively, indicating that these structures are more stable than their neighboring clusters. It is noteworthy that the binding energies of the studied $Mg_{n+1}$ and $Mg_nX$ clusters decrease in the sequence $Mg_nNi > Mg_nFe > Mg_nCo > Mg_nMg$, except for the $Mg_6Fe$ and $Mg_6Co$ clusters. This indicates that $Mg_n$ cluster stability is enhanced by doping the cluster with Fe, Co, and Ni atoms in sequence. Figure 3 shows the fragmentation energies and the second-order differences in energy of $Mg_nX$ clusters. The results for bare $Mg_n$ clusters agree with those given in a previous work by Lyalin et al. [13]. For $Mg_nFe$ and $Mg_nCo$ clusters, the fragmentation energies and the second-order differences in energy show an alternating even–odd phenomenon as the cluster size increases. This indicates that the clusters with even numbers of atoms are more stable than their neighboring clusters with odd numbers of atoms. There are three visible peaks in the curve at $n$=4 and 8 for $Mg_nFe$ and $n$=4 for $Mg_nCo$, which hint that the $Mg_4Fe$, $Mg_8Fe$, and $Mg_4Co$ clusters may be the most stable structures. For $Mg_nNi$ clusters, the local maxima in the fragmentation energy and the second-order differences in energy are located at $n$=2, 5 and $n$=2, 4, 8, respectively. This means that $Mg_4X$ clusters are more stable than their neighbors, which is in line with the results for the average binding energy. This trend in stability could be due to a geometric effect in which the stability is determined predominantly by the number of atoms rather than by the number of electrons. In other words, the cluster is stabilized as it can form a compact symmetric structure with enhanced stability. In fact, as discussed above, $Mg_4X$ (X = Fe, Co, Ni) clusters have high symmetry ($C_{2v}$, $C_{2v}$, $T_d$).

## Electronic properties

The HOMO–LUMO gap is usually considered a measure of the kinetic stability of a compound. A larger gap indicates that the compound is inert with respect to chemical reactivity. The HOMO–LUMO gaps are displayed in Fig. 4 for $Mg_nX$ (X = Fe, Co, Ni, $n$=1–9) clusters. As can be seen, the HOMO–LUMO gaps for the most stable $Mg_nX$ (X = Fe, Co, Ni, $n$=1–9) clusters range from 0.610 to 2.479 eV. However, they are smaller than those of the corresponding $Mg_{n+1}$ clusters (1.605–3.284 eV). Although the HOMO–LUMO energy gap does not correlate directly with the fragmentation energy and second-order difference in energy, one can see from Fig. 4 that the curves of the HOMO–LUMO gaps show similar trends to those of the fragmentation energies and the second-order differences in energy of $Mg_nX$ (X = Fe, Co, Ni, $n$=1–9) clusters. Evidently, the HOMO–LUMO gaps of the various $Mg_nX$ (X = Fe, Co, Ni, $n$=1–9)

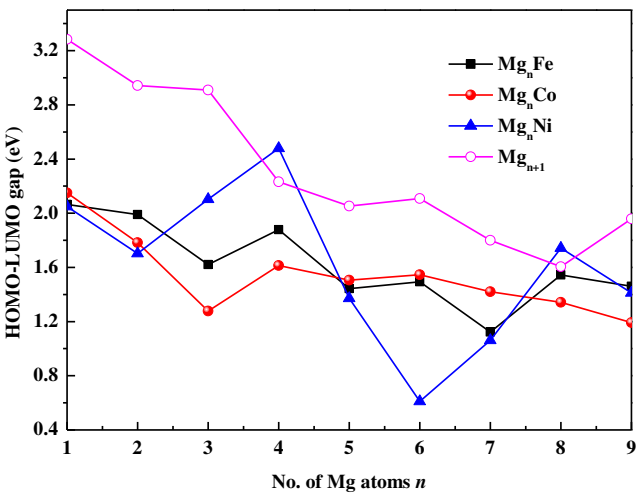


**Fig. 4** Size dependence of the HOMO–LUMO gaps of $Mg_{n+1}$ and $Mg_nX$ (X = Fe, Co, Ni, $n$=1–9) clusters

Author's personal copy



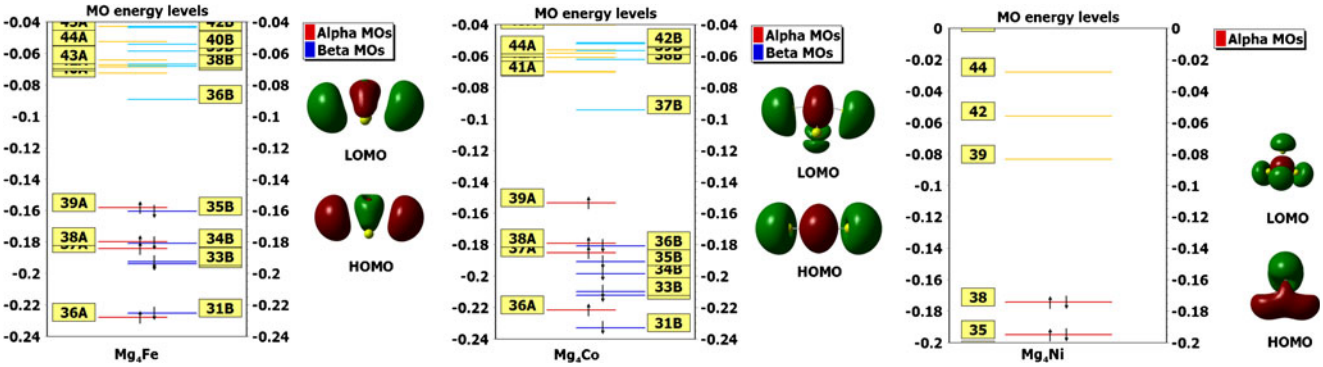


**Fig. 5** Calculated molecular energy levels of $Mg_4X$ (X = Fe, Co, Ni) clusters, together with molecular orbital contour maps of the HOMOs and LUMOs

clusters reach a maximum at $n$=4, confirming the relatively high chemical stabilities of those clusters.

In light of the phenomenon that the $Mg_4X$ (X = Fe, Co, Ni) clusters are the most stable of the $Mg_nX$ (X = Fe, Co, Ni, $n$= 1–9) clusters, the molecular energy levels and orbital contour maps for the HOMO and LUMO were obtained and are displayed in Fig. 5. This figure shows that the molecular orbitals are split for the $Mg_4Fe$ and $Mg_4Co$ clusters, while they are not split at all for the $Mg_4Ni$ cluster. The chemical bonding associated with the HOMOs and LUMOs can be analyzed via the contributions of the different atomic orbital components ($s$, $p$, $d$) to the molecular orbital. A systematic

**Table 3** Natural populations of X atoms, natural electron configurations of X and Mg atoms, and Wiberg bond indices (WBI) of Mg–X and Mg–Mg bonds for $Mg_nX$ clusters

| $Mg_nX$ | $n$ | $Q$(X) | NEC(X) | NEC(Mg) | WBI(Mg–X) | WBI(Mg–Mg) |
|---|---|---|---|---|---|---|
| X = Fe | 1 | −0.16571 | $4s^{1.17}3d^{6.93}4p^{0.06}4d^{0.01}$ | $3s^{1.64}3p^{0.19}$ | 0.49 | – |
| | 2 | −0.35967 | $4s^{1.12}3d^{6.94}4p^{0.29}4d^{0.01}$ | $3s^{1.63}3p^{0.19}4s^{0.01}$ | 0.51 | 0.18 |
| | 3 | −0.39609 | $4s^{1.26}3d^{6.95}4p^{0.15}4d^{0.03}$ | $3s^{1.57–1.79}3p^{0.13–0.30}$ | 0.06–0.51 | 0.02–0.32 |
| | 4 | −0.87266 | $4s^{1.09}3d^{6.94}4p^{0.79}4d^{0.04}5p^{0.02}$ | $3s^{1.26–1.37}3p^{0.41–0.51}4p^{0.01}$ | 0.54–0.65 | 0.10–0.47 |
| | 5 | −2.23862 | $4s^{1.09}3d^{7.20}4p^{1.88}4d^{0.07}$ | $3s^{1.27–1.28}3p^{0.24–0.37}4p^{0.01}$ | 0.66–0.92 | 0.05–0.15 |
| | 6 | −2.81683 | $4s^{0.94}3d^{7.64}4p^{2.15}5s^{0.01}4d^{0.09}$ | $3s^{1.10–1.11}3p^{0.24–0.45}4p^{0.01}$ | 0.66–0.82 | 0.10–0.24 |
| | 7 | −2.94868 | $4s^{1.19}3d^{7.36}4p^{2.30}5s^{0.01}4d^{0.09}5p^{0.01}$ | $3s^{0.99–1.14}3p^{0.40–0.60}4p^{0.01}$ | 0.55–0.74 | 0.06–0.31 |
| | 8 | −4.20885 | $4s^{1.13}3d^{7.84}4p^{3.06}4d^{0.18}$ | $3s^{0.98}3p^{0.49}4p^{0.01}$ | 0.65 | 0.05–0.15 |
| | 9 | −3.91102 | $4s^{1.04}3d^{7.71}4p^{3.04}4d^{0.12}$ | $3s^{0.95–1.37}3p^{0.31–0.71}4p^{0.01–0.02}$ | 0.12–0.63 | 0.02–0.34 |
| X = Co | 1 | −0.20729 | $4s^{1.17}3d^{7.98}4p^{0.04}$ | $3s^{1.61}3p^{0.18}$ | 0.49 | – |
| | 2 | −0.47106 | $4s^{1.28}3d^{8.01}4p^{0.16}4d^{0.02}$ | $3s^{1.63}3p^{0.13}$ | 0.42 | 0.08 |
| | 3 | −1.06033 | $4s^{0.81}3d^{8.58}4p^{0.63}4d^{0.03}$ | $3s^{1.50}3p^{0.04–0.18}4s^{0.01}4p^{0.00–0.01}$ | 0.71–0.77 | 0.06–0.15 |
| | 4 | −1.47307 | $4s^{1.10}3d^{8.11}4p^{1.23}5s^{0.01}4d^{0.03}5p^{0.01}$ | $3s^{1.27–1.35}3p^{0.27–0.36}4p^{0.01}$ | 0.63–0.76 | 0.06–0.34 |
| | 5 | −2.97620 | $4s^{1.12}3d^{8.56}4p^{2.22}5s^{0.01}4d^{0.07}$ | $3s^{1.13–1.20}3p^{0.24–0.30}$ | 0.73–0.94 | 0.07–0.12 |
| | 6 | −4.81354 | $4s^{1.06}3d^{9.47}4p^{3.25}4d^{0.04}$ | $3s^{0.91}3p^{0.29}$ | 0.73 | 0.06–0.08 |
| | 7 | −4.05675 | $4s^{0.95}3d^{9.07}4p^{3.00}4d^{0.04}$ | $3s^{0.93–1.40}3p^{0.24–0.51}4p^{0.00–0.01}$ | 0.20–0.84 | 0.04–0.45 |
| | 8 | −2.28721 | $4s^{1.05}3d^{8.13}4p^{2.06}5s^{0.01}4d^{0.04}5p^{0.01}$ | $3s^{1.06–1.40}3p^{0.30–0.80}4p^{0.01–0.02}$ | 0.17–0.65 | 0.04–0.47 |
| | 9 | −1.28865 | $4s^{0.93}3d^{8.04}4p^{1.29}5s^{0.01}4d^{0.02}5p^{0.01}$ | $3s^{1.02–1.16}3p^{0.49–1.08}4s^{0.01–0.03}4p^{0.03}$ | 0.12–0.52 | 0.03–0.44 |
| X = Ni | 1 | −0.23183 | $4s^{1.18}3d^{9.01}4p^{0.04}$ | $3s^{1.59}3p^{0.18}$ | 0.49 | – |
| | 2 | −0.54488 | $4s^{1.39}3d^{8.97}4p^{0.17}4d^{0.02}$ | $3s^{1.61}3p^{0.12}$ | 0.42 | 0.09 |
| | 3 | −1.48260 | $4s^{0.77}3d^{9.81}4p^{0.89}5p^{0.01}$ | $3s^{1.38}3p^{0.13}$ | 0.81 | 0.15 |
| | 4 | −2.92793 | $4s^{0.97}3d^{9.89}4p^{2.06}5p^{0.01}$ | $3s^{1.14}3p^{0.13}$ | 0.97 | 0.09 |
| | 5 | −3.60678 | $4s^{1.14}3d^{9.82}4p^{2.62}5s^{0.01}4d^{0.01}$ | $3s^{0.99–1.10}3p^{0.24–0.27}$ | 0.73–0.99 | 0.06–0.10 |
| | 6 | −4.79247 | $4s^{1.47}3d^{9.82}4p^{3.48}5s^{0.02}$ | $3s^{0.97}3p^{0.23}$ | 0.81 | 0.07–0.13 |
| | 7 | −4.27623 | $4s^{1.11}3d^{9.85}4p^{3.32}$ | $3s^{0.88–1.48}3p^{0.25–0.53}4p^{0.01}$ | 0.10–0.70 | 0.00–0.45 |
| | 8 | −3.87364 | $4s^{0.93}3d^{9.87}4p^{3.07}$ | $3s^{0.97–1.39}3p^{0.22–0.68}4p^{0.00–0.02}$ | 0.14–0.81 | 0.06–0.37 |
| | 9 | −3.76145 | $4s^{0.95}3d^{9.73}4p^{3.07}4d^{0.02}$ | $3s^{0.86–1.17}3p^{0.38–0.81}4p^{0.01–0.02}$ | 0.15–0.61 | 0.02–0.38 |

Author's personal copy



analysis reveals that the HOMOs and LUMOs of the $Mg_4Fe$ and $Mg_4Co$ clusters are very similar. For the $Mg_4Fe$ and $Mg_4Co$ clusters, the HOMO involves the 3*s* and $3p_z$ orbitals from the Mg atoms and the 4*s*, $3d_{x^2-y^2}$, and $3d_{z^2}$ orbitals from the Fe and Co atoms, whereas the LUMO mostly involves the 3*s* and $3p_z$ orbitals of the Mg atoms as well as the 4*s*, $3d_{x^2-y^2}$, and $3d_{z^2}$ orbitals of the Fe and Co atoms. However, for the $Mg_4Ni$ cluster, the HOMO mainly comes from the 3*s* and 3*p* orbitals of Mg and the $4p_y$ and $3d_{xz}$ orbitals of Ni, whereas the 3*s*, $3p_x$, $3p_y$, and $3p_z$ orbitals of Mg and the 4*s* orbital of Ni are the main contributors to the LUMO. These molecular orbitals indicate the presence of *spd* hybridization of the X atom and *sp* hybridization of the Mg atoms.

## Population analysis

Natural population analysis (NPA) provides a reasonable explanation of the charge transfer within the cluster. The results of NPA for the lowest-energy $Mg_nX$ (X = Fe, Co, Ni, $n$=1–9) clusters are summarized in Table 3. NPA shows that, overall, the X atom always gains electrons from its neighboring Mg atoms, and is therefore negatively charged. In the ground-state isomers, the charge on the X atom is −4.81354*e* to −0.16571*e* for $n$=1–9. This can be attributed to the higher electronegativity of the X atoms than the Mg atom. In order to gain a detailed understanding of the charge transfer, the natural electron configurations (NECs) for the most stable $Mg_nX$ systems were investigated (the results are tabulated in Table 3). It was found that the 4*s*, 3*d*, and 4*p* orbitals of the X atoms behave predominantly as core orbitals, while the 4*d*, 5*s*, and 5*p* states make only weak contributions. The valence electron configurations of the free Fe, Co, and Ni atoms are $3d^64s^2$, $3d^74s^2$, and $3d^84s^2$, respectively. When the X and Mg atoms combine to form the $Mg_nX$ (X = Fe, Co, Ni, $n$=1–9) clusters, the NPA results illustrate that the valence electron configurations change to $4s^{0.94-1.26}3d^{6.93-7.84}4p^{0.06-3.06}$ (for Fe), $4s^{0.81-1.28}3d^{7.98-9.47}4p^{0.04-3.25}$ (for Co), and $4s^{0.77-1.47}3d^{8.97-9.89}4p^{0.04-3.48}$ (for Ni). Strong *spd* hybridization stemming from electron transfer from the 3*s* orbitals of the Mg atoms and the 4*s* orbital of the X atom to the 3*d* and 4*p* atomic orbitals of the X atom is observed in the $Mg_nX$ clusters. The stabilities of the $Mg_nX$ (X = Fe, Co, Ni, $n$=1–9) clusters are mainly enhanced by direct electron transfer from the Mg atoms to the X atom due to electronegativity differences. In the MgFe, MgCo, and MgNi dimers, all of the Mg–X single bonds have a Wiberg bond index (WBI) of 0.49. However, the WBI values for the Mg–X and Mg–Mg bonds in the $Mg_nX$ clusters are small, which indicates that the Mg–X and Mg–Mg bonds are weak single bonds. In addition, the WBIs of the Mg–X bonds (0.06–0.99) are generally larger than those of the Mg–Mg bonds (0.02–0.47). Therefore, the interactions between Mg and X atoms are generally stronger than the Mg–Mg interactions.

## Magnetic properties

The total magnetic moments of the studied $Mg_{n+1}$ and $Mg_nX$ (X = Fe, Co, Ni; $n$=1–9) clusters as well as the local magnetic moments of Fe, Co, and Ni atoms in $Mg_nX$ clusters are plotted as a function of cluster size in Fig. 6. The local magnetic moments of open 3*d* transition metals gradually decrease in the order Fe > Co > Ni, which is in accord with the gradual reduction in the number of unpaired 3*d* electrons. For the pure $Mg_{n+1}$ systems, the magnetic moments are zero, because two 3*s* electrons are paired. When an Mg atom in an $Mg_{n+1}$ cluster is replaced with an Fe, Co, or Ni atom, the resulting $Mg_nX$ (X = Fe, Co, Ni) cluster may possess a magnetic moment. In particular, $Mg_nFe$ clusters (except for $n$=7) have the largest magnetic moments (4 $\mu_B$). The $Mg_7Fe$ cluster has the smallest atomic magnetic moment of 2 $\mu_B$ among the $Mg_{1-9}Fe$ clusters. For the $Mg_nFe$ clusters, the total magnetic moment is mainly located on the Fe atom. The irregularity in the trend in the magnetic moments of these clusters at $n$=7 is due to the fact that the most stable structure of $Mg_7Fe$ possesses triplet spin multiplicity. The magnetic moments of the $Mg_nCo$ isomers are 3 $\mu_B$ except for the $Mg_3Co$ and $Mg_7Co$ isomers, which have magnetic moments of 1 $\mu_B$. The magnetic moments of the $Mg_{3,7}Co$ clusters are mainly located on the Co atom. The ground-state structures of the

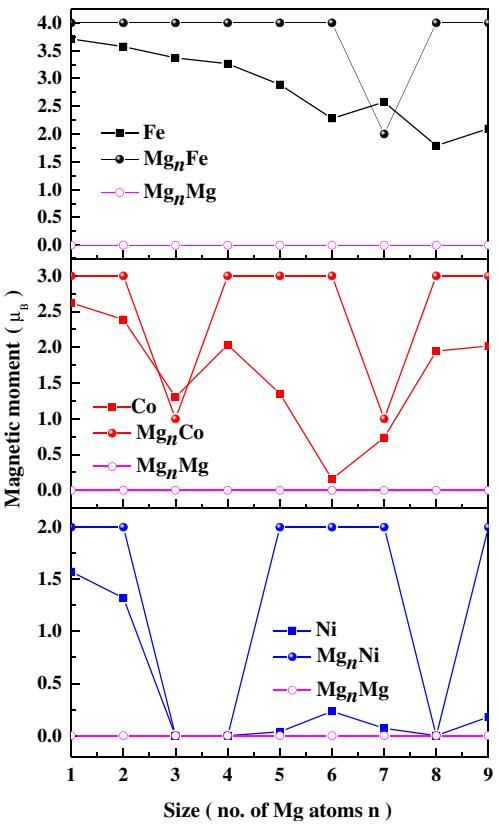


**Fig. 6** Total magnetic moments of the $Mg_nX$ (X = Fe, Co, Ni, Mg, $n$=1–9) clusters and local magnetic moments of the Fe, Co, and Ni atoms

Author's personal copy



$Mg_{3,7}Co$ clusters possess doublet spin multiplicity. It can be seen in Fig. 6 that the magnetic moments of $Mg_{1,2,5,6,7,9}Ni$ clusters are 2 $\mu_B$. However, the magnetic moments of $Mg_{3,4,8}Ni$ clusters are quenched. The magnetic moments of $Mg_{3,4,8}Ni$ clusters are due to the local magnetic moment of the Ni atom. The 3*d* valence shell of the Ni atom is fully filled and the local magnetic moment of Ni is zero according to the natural population. Therefore, the magnetic moments of $Mg_nNi$ clusters are quenched for $Mg_nNi$ ($n$=3, 4, and 8).

## Conclusions

In summary, the growth behavior, stabilities, and the electronic and magnetic properties of $Mg_nX$ (X = Fe, Co, Ni) clusters were studied systematically using DFT based on the generalized gradient approximation. It was found that the $Mg_nFe$, $Mg_nCo$, and $Mg_nNi$ clusters have similar geometric structures and that the X atom is endohedrally localized in $Mg_nX$ clusters. The stabilities of the ground-state structures of these clusters were examined by analyzing the average atomic binding energies, fragmentation energies, second-order differences in energy, and the HOMO–LUMO gaps, and the results show that $Mg_4X$ clusters are relatively stable. Results from natural population analysis (NPA) showed that the dopant atom (Fe, Co, or Ni) acts as an electron acceptor due to its high electronegativity relative to that of the Mg atom. The strong *spd* hybridizations observed in the $Mg_nX$ clusters stems from electron transfer from the 3*s* orbitals of the Mg atoms and the 4*s* orbital of the X atom to the 3*d* and 4*p* atomic orbitals of the X atom. Moreover, the spin magnetic moments were analyzed and compared. Various clusters, such as $Mg_{1,2,3,4,5,6,8,9}Fe$, $Mg_{1,2,4,5,6,8,9}Co$, and $Mg_{1,2,5,6,7,9}Ni$, present high magnetic moments of 4 $\mu_B$, 3 $\mu_B$, and 2 $\mu_B$, respectively. However, the $Mg_7Fe$, $Mg_{3,7}Co$, and $Mg_{3,4,8}Ni$ clusters have low magnetic moments of 2 $\mu_B$, 1 $\mu_B$, and 0, respectively.

**Acknowledgments** This project was supported by the Natural Science Foundation of the Higher Education Institutions of Jiangsu Province (grant no. 13KJB140018), the foundation of the Yancheng Institute of Technology (grant nos. XKR2011023 and XKY2013014), the research fund of the Key Laboratory for Advanced Technology in Environmental Protection of Jiangsu Province (grant nos. AE201128 and AE201313), the research fund of the Open Project of Key Laboratory for Ecological-Environment Materials of Jiangsu Province (grant no. EML2012011), the Education Department of Sichuan Province (grant no. 11ZB099), and the research fund of the Sichuan University of Science and Engineering (grant no. 2012PY16)

## References

1. Larsson P, Araújo CM, Larsson JA, Jena P, Ahuja R (2008) Proc Natl Acad Sci 105:8227–8231
2. Liang G, Huot J, Boily S, Van Neste A, Schulz R (1999) J Alloys Compd 292:247–252
3. Khrussanova M, Grigorova E, Mitov I, Radev D, Peshev P (2001) J Alloys Compd 327:230–234
4. Reuse F, Khanna SN, de Coulon V, Buttet J (1990) Phys Rev B 41: 11743–11759
5. Kumar V, Car R (1991) Phys Rev B 44:8243–8255
6. Gong XG, Zheng QQ, He Y-Z (1993) Phys Lett A 181:459–464
7. Sanabria SJ, Hilbers U, Neuenschwander J, Niemz P, Sennhauser U, Thoemen H, Wenker JL (2013) Ultrasonics 53:157–170
8. Akola J, Rytkönen K, Manninen M (2001) Eur Phys J D 16:21–24
9. Diederich T, Döppner T, Braune J, Tiggesbäumker J, Meiwes-Broer K-H (2001) Phys Rev Lett 86:4807–4810
10. Kohn A, Weigend F, Ahlrichs R (2001) Phys Chem Chem Phys 3: 711–719
11. Thomas OC, Zheng W, Xu S, Bowen KH Jr (2002) Phys Rev Lett 89: 213403
12. Acioli PH, Jellinek J (2002) Phys Rev Lett 89:213402
13. Lyalin A, Solov'yov IA, Solov'yov AV, Greiner W (2003) Phys Rev A 67:063203
14. Diederich T, Döppner T, Fennel T, Tiggesbäumker J, Meiwes-Broer KH (2005) Phys Rev A 72:023203
15. Heidari I, De S, Ghazi SM, Goedecker S, Kanhere DG (2011) J Phys Chem A 115:12307–12314
16. Medel VM, Reber AC, Reveles JU, Khanna SN (2012) J Chem Phys 136:134311–134318
17. Becke AD (1988) Phys Rev A 38:3098–3100
18. Perdew JP, Wang Y (1992) Phys Rev B 45:13244–13249
19. Krishnan R, Binkley JS, Seeger R, Pople JA (1980) J Chem Phys 72: 650–654
20. Blaudeau J-P, McGrath MP, Curtiss LA, Radom L (1997) J Chem Phys 107:5016–5021
21. Glukhovtsev MN, Pross A, McGrath MP, Radom L (1995) J Chem Phys 103:1878–1885
22. Ruette F, Sánchez M, Añez R, Bermúdez A, Sierraalta A (2005) J Mol Struct THEOCHEM 729:19–37
23. Huber KP, Herzberg G (1979) Molecular spectra and molecular structure IV. Constants of diatomic molecules. Van Nostrand Reinhold, New York
24. Moskovits M, DiLella DP, Limm W (1984) J Chem Phys 80:626–633
25. Purdum H, Montano PA, Shenoy GK, Morrison T (1982) Phys Rev B 25:4412–4417
26. Cox DM, Trevor DJ, Whetten RL, Rohlfing EA, Kaldor A (1985) Phys Rev B 32:7290–7298
27. Montano PA, Shenoy GK (1980) Solid State Commun 35:53–56
28. Lian L, Su CX, Armentrout PB (1992) J Chem Phys 97: 4072–4083
29. Loh SK, Lian L, Hales DA, Armentrout PB (1988) J Phys Chem 92: 4009–4012
30. Moskovits M, DiLella DP (1980) J Chem Phys 73:4917–4924
31. Kant A, Strauss B (1964) J Chem Phys 41:3806–3808
32. Leopold DG, Lineberger WC (1986) J Chem Phys 85:51–55
33. Dong J-G, Hu Z, Craig R, Lombardi JR, Lindsay DM (1994) J Chem Phys 101:9280–9282
34. Morse MD, Hansen GP, Langridge-Smith PRR, Zheng L-S, Geusic ME, Michalopoulos DL, Smalley RE (1984) J Chem Phys 80:5400–5405
35. Pinegar JC, Langenberg JD, Arrington CA, Spain EM, Morse MD (1995) J Chem Phys 102:666–674
36. Moskovits M, Hulse JE (1977) J Chem Phys 66:3988–3994
37. Ahmed F, Nixon ER (1979) J Chem Phys 71:3547–3549
38. Wang H, Haouari H, Craig R, Lombardi JR, Lindsay DM (1996) J Chem Phys 104:3420–3422
39. Fuyang T, Yuanxu W, Qun J, Kai T, Youhua L (2008) Acta Phys Sin 57:1648–1655

Author's personal copy



40. Frisch MJ, Schlegel HB, Scuseria GE, Robb MA, Cheeseman JR, Scalmani G, Barone V, Mennucci B, Petersson GA, Nakatsuji H, Caricato M, Li X, Hratchian HP, Izmaylov AF, Bloino J, Zheng G, Sonnenberg JL, Hada M, Ehara M, Toyota K, Fukuda R, Hasegawa J, Ishida M, Nakajima T, Honda Y, Kitao O, Nakai H, Vreven T, Montgomery JA Jr, Peralta JE, Ogliaro F, Bearpark M, Heyd JJ, Brothers E, Kudin KN, Staroverov VN, Kobayashi R, Normand J, Raghavachari K, Rendell A, Burant JC, Iyengar SS, Tomasi J, Cossi M, Rega N, Millam JM, Klene M, Knox JE, Cross JB, Bakken V, Adamo C, Jaramillo J, Gomperts R, Stratmann RE, Yazyev O, Austin AJ, Cammi R, Pomelli C, Ochterski JW, Martin RL, Morokuma K, Zakrzewski VG, Voth GA, Salvador P, Dannenberg JJ, Dapprich S, Daniels AD, Farkas O, Foresman JB, Ortiz JV, Cioslowski J, Fox DJ (2009) Gaussian 09. Gaussian Inc., Wallingford